Scattering-Based Geometric Shaping of Photon-Photon Interactions

Shahaf Asban and Shaul Mukamel

Scattering-based geometric shaping of photon-photon interactions

Shahaf Asban[1, *] and Shaul Mukamel[1, †]

[1]*Department of Chemistry and Physics and Astronomy,*
University of California, Irvine, California 92697-2025, USA

We construct an effective Hamiltonian of interacting bosons, based on scattered radiation off vibrational modes of designed molecular architectures. Making use of the infinite yet countable set of spatial modes representing the scattering of light, we obtain a variable photon-photon interaction in this basis. The effective Hamiltonian hermiticity is controlled by a geometric factor set by the overlaps of spatial modes. Using this mapping, we relate intensity measurements of the light to correlation functions of the interacting bosons evolving according to the effective Hamiltonian, rendering local as well as nonlocal observables accessible. This architecture may be used to simulate the dynamics of interacting bosons, as well as designing tool for multi-qubit photonic gates in quantum computing applications. Variable hopping, interaction and confinement of the active space of the bosons are demonstrated on a model system.

Quantum machines are fundamentally different from their classical counterparts [1]. Classical computers are implemented using a binary basis set. One of the benefits of this choice is minimal average energy consumption [2] as well as minimal bit error rate in the information transmission of a noisy channel [3]. For such a machine to be useful, it requires large scale integration of fundamental operations, where each level adds to the overall error rate. Deterministic intermediate quantities can be measured and corrected via feedback loops without interrupting the calculation process. In quantum machines the smallest possible unit of data (qubit) carries a phase which manifests a continuous degree of freedom. Upscaling of operations on qubits is also required for nontrivial tasks. The propagation of quantum information through such integrated system evolves errors continuously as well. This makes the realization of fault tolerant quantum processing challenging, and continues to motivate intense scientific effort [4–6]. Quantum simulators based on optical traps pioneered by Cirac and Zoller [7, 8] have matured experimentally [9, 10]. They are widely used in the study of quantum dynamics such as spin frustration [10] and thermalization and localization transitions [11, 12]. Recently more applications of lattice gauge theories have been proposed, appealing to simulations of high energy physics [13–15]. While these fascinating quantum simulators offer unprecedented glimpse into nonequilibrium dynamics, upscaling the number of qubits is just as challenging.

Here we propose a Geometric scattering-based Spatial Photon Coupler (SPC) that can be used to simulate quantum dynamics of interacting bosons. The setup is depicted in Fig.(1), and based on *off-resonant scattering* of photons on geometrically arranged distribution of molecules. We show that the scattering process can be mapped into the effective Hamiltonian,

$$H_{eff} = \sum_{nk} \Theta_{nk} a_n^\dagger a_k - \sum_{nklm} U_{nklm} a_n^\dagger a_k a_l^\dagger a_m, \quad (1)$$
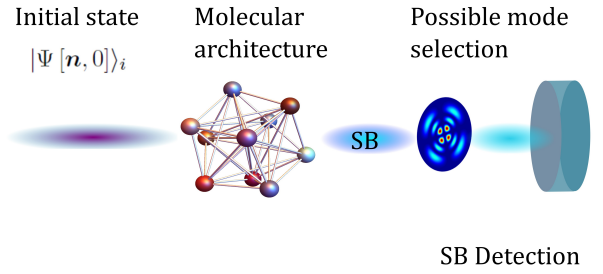

FIG. 1. *Proposed realization of the geometric SPC.* The incident beam is scattered-off a molecular architecture, realizing interaction between its spatial components denoted SB. A single mode as well as any combination of such are addressable, rendering projective measurement in the chosen basis possible. The SBs can be mapped into discrete lattice sites for which cross-correlations can be constructed using the photon-statistics.

where $a_k \left(a_k^\dagger\right)$ is a discrete bosonic annihilation (creation) operator. The hopping (Θ_{nk}) and the interaction (U_{nklm}) terms are determined by three main quantities: (1) the geometry (design) of the microscopic building blocks (2) their internal structure (spectrum) (3) the measurement basis chosen. It holds two significant advantages. First, it can be designed to maintain hermiticity such that marginal losses in photon number occur [16], inelastic contributions in this case result in frequency shift of the incident photon. Second, while the number of connected modes is infinite, it can be confined with intelligent design. Our goal is to shape the induced dynamics constrained by the Hamiltonian in Eq.(1) then read the encoded information from the final photonic wavefunction,

$$|\Psi[\boldsymbol{n}, \tau]\rangle_f = e^{-iH_{eff}\tau}|\Psi[\boldsymbol{n}, 0]\rangle_i. \quad (2)$$

Intensity measurements reveal the Scattered Bosons (SBs) densities $\hat{n}_k \equiv a_k^\dagger a_k$, evolving on a network (graph) of a topology imposed by H_{eff} connectivity as depicted

in Fig.(1). τ denotes the interaction time, beyond which $U_{nklm} \equiv 0$.

We consider arbitrary initial superposition of spatial modes, reflecting some initial (multiple-photon) distribution of SBs. One possibility of particular interest to the simulation of interacting bosons, is a (normalized) product of N single photon states $|\mathbf{1}\rangle = \sum_n \mathcal{C}_n a_n^\dagger |0\rangle$, corresponding to initially noninteracting bosons. One way to achieve that is by direct state preparation. Another is via two-mode spontaneous parametric down converter source in which one photon is scattered while the other serves as the Reference for the SB (RSB) as was done in [17] and inspired by [18–22], see [23]. In both manifestations, the RSBs are used to extract the SBs statistics which is first scattered as depicted in Fig (1). Surveying the SBs statistics using cross-correlations with RSBs, renders "local" $\propto \langle \hat{n}_r(\tau) \rangle$ and $\langle \hat{n}_r(0)\hat{n}_r(\tau) \rangle$, as well as "nonlocal" quantities $\propto \sum_R \langle \hat{n}_r(0)\hat{n}_{r+R}(\tau) \rangle$ accessible. While conventional quantum simulators are limited by the number of physical qubits, the proposed geometric SPC benefits from controlled - potentially infinite - number of participating modes. These characteristics are highly desirable for simulating thermodynamic properties of interacting particles.

Constructing the effective Hamiltonian. Off-resonant light-matter interaction is given by the minimal coupling Hamiltonian,

$$H_{\mu\phi} = \int d\mathbf{r}\, \sigma(\mathbf{r},t)\, \mathbf{A}^2(\mathbf{r},t), \qquad (3)$$

where μ and ϕ denote the matter and photon fields respectively. Radiation modes interaction is mediated by the charge-density operator $\sigma(\mathbf{r})$. The vector potential in the paraxial approximation takes the form $\mathbf{A}_p(\mathbf{r},t) = \sum_{\sigma,l,p} \int_0^\infty dk_0 C(k_0)\left[A_{\sigma lp}^{(+)}(k_0)e^{ik_0(z-ct)} + h.c.\right]$, where k_0 is the wavevector in the longitudinal direction, $C(k_0) = \left(1+\vartheta^2/16\pi^3\varepsilon_0 k_0\right)^{1/2}$ and $\vartheta = q/\sqrt{2k_0^2}$ is the degree of paraxiality [24, 25]. The vector potential operator is defined by $A_{\sigma lp}^{(+)}(k_0) = \epsilon_\sigma \hat{a}_{\sigma,l,p}(k_0)\psi_{l,p}(\boldsymbol{\rho},z;k_0)$ where $\hbar = c = 1$. $\boldsymbol{\rho}$ is the polar distance (cylindrical coordinates) and the indices l,p label the spatial basis set $\psi_{lp}(\boldsymbol{\rho},z;k_0)$ [in [24, 25] Laguerre-Gauss (LG) basis is used]. Any complete basis which is a solution of the paraxial equation, such as Hermite- or Ince-Gauss (HG,IG) can be used. Here $\epsilon_\sigma = (\mathbf{u}_x - i\sigma\mathbf{u}_y)/\sqrt{2}$ is the polarization vector [circular for LG modes (linear for HG)] and $\sigma = \pm 1$. The field (creation/annihilation) operators in the paraxial basis satisfy the canonical commutation relations, $\left[\hat{a}_{\sigma,l,p}(k_0), \hat{a}_{\sigma',l',p'}^\dagger\left(k_0'\right)\right] = \delta_{\sigma\sigma'}\delta_{ll'}\delta_{pp'}\delta\left(k_0 - k_0'\right)$. The paraxial basis is given by the transformation of the standard operators $\hat{a}_{\sigma,l,p}(k_0) = \int d^2\mathbf{q}\phi_{lp}^*(\mathbf{q})\hat{a}_\sigma(\mathbf{q})$. This basis has the following properties,

$$\sum_{l,p} \phi_{lp}^*(\mathbf{q})\psi_{lp}(\boldsymbol{\rho},z,k_0) = e^{i\mathbf{q}\cdot\boldsymbol{\rho} - k_0\vartheta^2 z} \qquad (4a)$$

$$\int d^2\mathbf{q}\phi_{lp}^*(\mathbf{q})\phi_{mn}(\mathbf{q}) = \delta_{lm}\delta_{pn} \qquad (4b)$$

$$\sum_{l,p} \phi_{lp}^*(\mathbf{q})\phi_{lp}(\mathbf{q}') = \delta(\mathbf{q} - \mathbf{q}') \qquad (4c)$$

where $\mathbf{q}$ is the transverse momentum and $\phi_{lp}(\mathbf{q})$ is the LG spatial modes Fourier transform taken at $z = 0$. The full Hamiltonian is given by $\mathcal{H} = H_0 + H_{\mu\phi}$, where $H_0 = H_\phi + H_\mu$ is the noninteracting Hamiltonian of the radiation (ϕ) and matter (μ). With these notations, the interaction Hamiltonian can be recast in the form,

$$H_{\mu\phi} = \sum_{\mathbf{k}\mathbf{q}} \sigma_{\mathbf{k}-\mathbf{q}}^\dagger a_{\mathbf{k}}^\dagger a_{\mathbf{q}} + \sigma_{\mathbf{k}-\mathbf{q}} a_{\mathbf{k}} a_{\mathbf{q}}^\dagger, \qquad (5)$$

where the highly oscillating terms corresponding to $a_{\mathbf{k}} a_{\mathbf{q}}$ and $a_{\mathbf{k}}^\dagger a_{\mathbf{q}}^\dagger$ are neglected. The matter Hamiltonian is given by $H_\mu = \sum_{\alpha,i} \epsilon_{i,\alpha} c_{i,\alpha}^\dagger c_{i,\alpha}$, where $c_{i,\alpha}\left(c_{i,\alpha}^\dagger\right)$ is the bosonic annihilation (creation) operator with the canonical commutation relations $\left[c_{i,\alpha}, c_{j,\beta}^\dagger\right] = \delta_{\alpha\beta}\delta_{i,j}$. The vibrational modes labeled i, and scatters by α. The charge-density operator reads $\sigma_{\mathbf{k}} = \sum_{\alpha=1}^N f_\alpha(\mathbf{k}) c_{i,\alpha}^\dagger c_{j,\alpha}$, where $f_\alpha(\mathbf{k}) = e^{i\mathbf{k}\cdot\mathbf{r}_\alpha} w(\mathbf{k})$, $w(\mathbf{k})$ are the localized molecular orbital and $\mathbf{r}_\alpha$ are scatterers positions. We then calculate the effective photon-photon interaction using the Schrieffer-Wolff transformation [see appendix (B.1) for detailed derivation], follows by a transformation of the momentum representation into superposition the SBs.

The SB representation. Using the above definitions for the Bogoliubov transformation from momentum space to the Schmidt representation $a_{\mathbf{k}} = \sum_n \phi_n(\mathbf{k}) a_n$, where a_n is the Schmidt boson annihilation operator and n is a shorthand notation for the two quantum numbers l, p introduced in the expression for the vector potential. The free Hamiltonian reads assuming a single longitudinal mode at ω_0 we get $H_\phi = \omega_0 \sum_n a_n^\dagger a_n$. The off-diagonal contributions to Eq.(1) - namely, the hopping terms - are given by (see appendix for detailed derivation),

$$\hat{t}_{coh} = \sum_{nm} \theta_{nm}^{coh} a_n^\dagger a_m + h.c., \qquad (6a)$$

$$\hat{t}_{inc} = \sum_{nm} \theta_{nm}^{inc}(\Delta_i) a_n^\dagger a_m + \theta_{nm}^{inc*}(-\Delta_i) a_m^\dagger a_n, \qquad (6b)$$

with the hopping coefficients are,

$$\theta_{nm}^{coh} = 2 \sum_{\alpha\neq\beta} \sum_{\mathbf{k},\mathbf{q},\mathbf{s}} e^{-i(\mathbf{k}-\mathbf{q})\cdot\mathbf{r}_\alpha + i(\mathbf{s}-\mathbf{q})\cdot\mathbf{r}_\beta} \qquad (7a)$$

$$\times \frac{\phi_n^*(\mathbf{k}) w_\alpha^*(\mathbf{k}-\mathbf{q}) w_\beta(\mathbf{s}-\mathbf{q}) \phi_m(\mathbf{s})}{q^2 - k^2},$$

$$\theta_{nm}^{inc}(\Delta_i) = 2 \sum_{\alpha} \sum_{\boldsymbol{k},\boldsymbol{q},\boldsymbol{s}} e^{-i(\boldsymbol{k}-\boldsymbol{s})\cdot\boldsymbol{r}_\alpha} \tag{7b}$$

$$\times \frac{\phi_n^*(\boldsymbol{k}) w_\alpha^*(\boldsymbol{k}-\boldsymbol{q}') w_\alpha(\boldsymbol{q}-\boldsymbol{q}') \phi_m(\boldsymbol{s})}{q'^2 - (k^2+\Delta_i)},$$

and $\Delta_i = 2\omega_0\epsilon_{ig}$. Assuming a slowly varying orbital in momentum domain (point particle limit), significantly simplifies Eqs.(7a, 7b). When the inter-particle distance is much smaller than the transverse wavevector $r_{\alpha\beta} \ll \lambda_\perp$, the coherent hopping [Eq.(7a)] is granted an intuitive form, carrying spatial contributions due to the phase-difference of scattered modes. Introducing a cutoff frequency Λ such that $|r_{\beta\alpha}|/\Lambda \le |r_{\beta\alpha}| k \ll 1$ and $q > 1/\Lambda$ we obtain,

$$\theta_{nm}^{coh} = g^{coh} \sum_{\alpha\neq\beta} \psi_n^*(\boldsymbol{r}_\alpha) \psi_m(\boldsymbol{r}_\beta), \tag{8a}$$

$$\theta_{nk}^{inc} = g^{inc} \sum_{\alpha} \psi_n^*(r_\alpha) \psi_k(r_\alpha). \tag{8b}$$

Note that these approximations are not essential yet grant important intuition; see appendix B for the exact expressions. The over-all SB hopping coefficient is given by $\Theta_{nk} = \omega_0 \left(\delta_{nk} - \theta_{nk}^{coh} - \theta_{nk}^{inc}\right)$.

The interaction term in Eq.(1) can be displayed in a form that separates the geometrical factor from the basis dependent one $U_{nmls} = -\sum_{l's'} S_{ll'ss'} V_{nml's'}$. Here V_{nlkm} is the basis dependent four-mode *scattering potential*,

$$V_{nlkm} = \sum_i \int d^2\boldsymbol{k} d^2\boldsymbol{q} \, \phi_n^*(\boldsymbol{k}) \phi_k(\boldsymbol{k}) \tag{9}$$

$$\times \left[\frac{1}{k^2-q^2-\Delta_i} - \frac{1}{k^2-q^2+\Delta_i}\right] \phi_l(\boldsymbol{q}) \phi_m^*(\boldsymbol{q}),$$

and the geometric structural tensor, $S_{ll'ss'} = \sum_\alpha f_{ll'}^{\alpha*} f_{ss'}^\alpha$, using concatenation of basis $\leftrightarrow$ geometry transformation $f_{nm}^\alpha = \psi_n^*(r_\alpha) \psi_m(r_\alpha)$ - isolating basis dependent properties from the geometric characteristics. The effective hamiltonian is finally given by Eq.(1).

The scattering potential in the Laguerre-Gauss basis. The target effective interaction to be simulated is manipulated and designed using three main ingredients. (i) One is purely geometric and defined by the arrangement of charges, (ii) the internal structure of each charge (Δ_i) and (iii) the choice of basis. While the geometric component appears in the expressions for both, the interaction and hopping terms, the charge spectral structure contributes to the scattering potential of Eq.(9) alone. We now study the effects of Δ on the interaction which is basis dependent yet geometry independent. The scattering
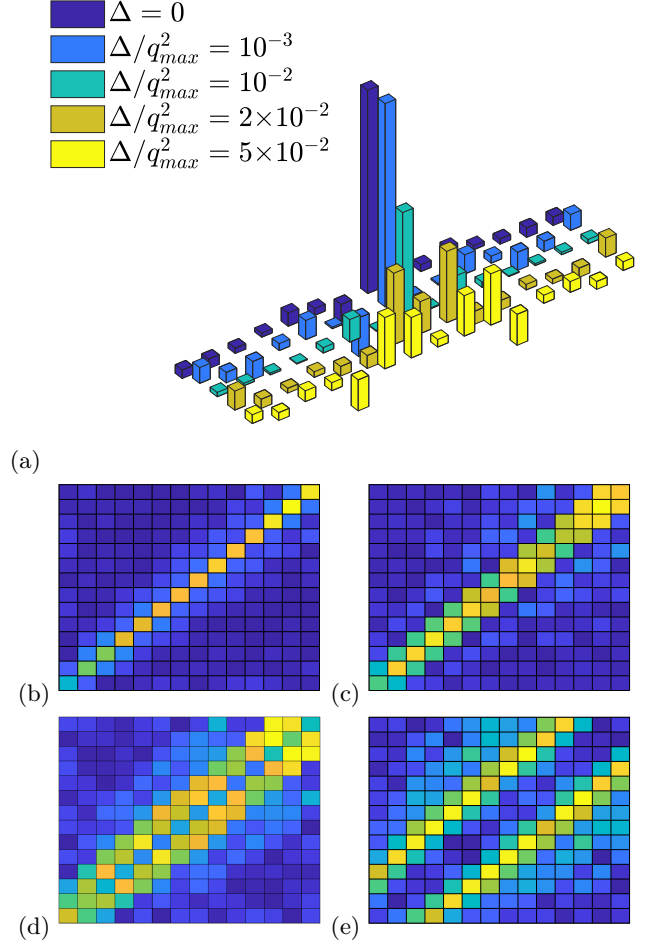

(a)

(b)   (c)

(d)   (e)

FIG. 2. *The scattering potential.* V_{nmkl} in Eq.(9) calculated in the LG basis. Each panel corresponds to different Δ value, and panel (a) captures a summary of the diagonal crossection from the top-left to bottom-right of panels b:e. Panels b:e capture the inter-mode coupling [relations between the two middle dimensions $(V_{mk} = tr_{nl} V_{nmkl})$], of the effective SBs scattering potential for the selected values $\Delta/q_{max}^2 = (0.001, 0.01, 0.02, 0.05)$. The calculated relations between the first two $(V_{nm} = tr_{kl} V_{nmkl})$ and last dimensions $(V_{kl} = tr_{nm} V_{nmkl})$ are indistinguishable from panel (b) for all values of Δ and resemble a Kronecker delta distribution.

potential V_{nklm} involves coupling between four modes. Eq.(9) can be further simplified using the LG basis [see Eq.(35B) of the supplementary material]. The structure of the scattering potential as a function of Δ for a two level system is depicted in Fig. (2). For all values of Δ, the relation between the first and last two modes [n,k and l,m of Eq.(1)] resembles a Kronecker delta . It is given by the partial traces $V_{nm} = tr_{kl} V_{nmkl} \approx \delta_{nm}$ and $V_{kl} = tr_{nm} V_{nmkl} \approx \delta_{kl}$ and depicted in Fig.(2a). This property simplifies the effective Hamiltonian to,

$$H_{eff}^{LG} = \sum_{n,k} \Theta_{nk} a_n^\dagger a_k - \sum_{nk} \mathcal{U}_{nk} \hat{n}_n \hat{n}_k, \tag{10}$$

where $\hat{n}_k = a_k^\dagger a_k$ is the number operator, and $\mathcal{U}_{nk} = \sum_{lm} U_{nlkm}\delta_{nl}\delta_{km}$. The effective potential between the first and last two modes of Eq.(1) spreads to neighboring modes with increasing values of Δ/q_{max}^2 where q_{max} is the cutoff wavevector in the numerical calculation. This behavior is summarized in Fig.(2a), and demonstrated separately for the selected values in Fig.(2b : e). At large values of Δ/q_{max}^2 the scattering occurs between more distant modes, corresponding to energy exchange with the matter. Extension of this result to a system of charges composed of a more complex internal structure, is given by a straightforward summation, resulting in longer-range interaction.

Illustrative example of the effective Hamiltonian. We derive the effective Hamiltonian for molecules in cylindrical architecture, in which controlled hopping can confine the dynamics to a restricted subspace. We consider a uniform distribution of molecules filling a hollow-cylinder (UC) of inner radius a and outer radius b as shown in Fig.(3). The boundary radius c is defined such that 95% of the power of the incident radial mode for which $n = 25$ is contained within the calculation range of the numerical simulation (the chosen cutoff mode).
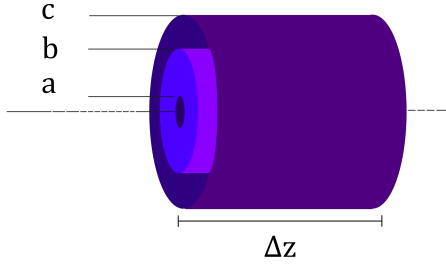

FIG. 3. *Uniformly distributed hollow-cylinder.* Inner and outer radius a and b respectively, c is chosen such that 95% of the power of the radial mode for which $n = 25$ is contained within. Δz is the region in which the interaction and hopping occur, corresponding to the interaction time interval τ.

In this case the geometric coefficient of the hopping terms in Eqs.(8a, 8b) as well as the interaction can be used to confine the dynamics in a controlled subspace. By varying a and b, the hopping range depicted in Figs.(4) a:d can be controlled. Fig.(4) along with Eqs.(8a, 8b) show that hopping within the set of modes corresponding to positive geometric factor, is energetically favorable. These positive contributions are surrounded by negative ones which are costly energetically, resulting in effective confinement. In this setup the single-molecule field scattering presented in Eq.(8b) dominates the hopping dynamics and the coherent hopping term of Eq.(8a) is suppressed. This is verified by the vanishing structure factor in a disordered lattice, or equivalently from the closure relations of the
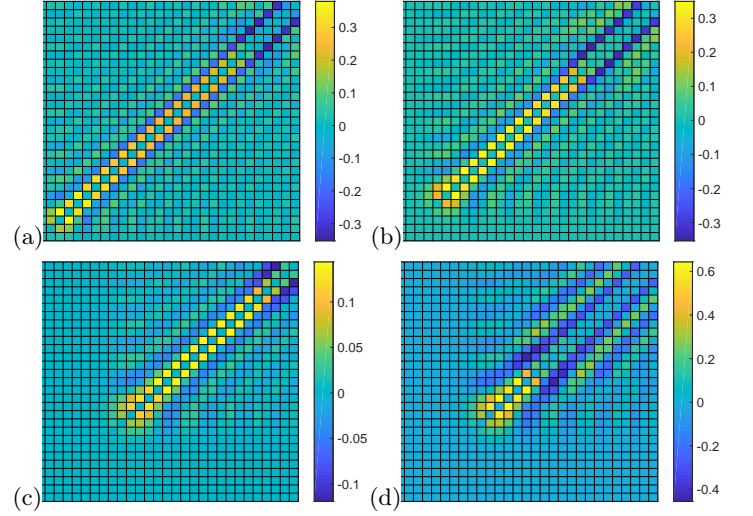

FIG. 4. *Geometrically controlled hopping confinement.* (a-d) The geometric hopping factors θ_{nk}^{inc} presented in Eq.(8b) are displayed for the above geometry. Panels a-d computed with the corresponding dimensionless distance from the origin $(a/c, b/c)$: [a $(0.1, 0.9)$, b $(0.2, 0.8)$, c $(0.4, 1)$, d $(0.4, 0.6)$]. Positive contributions are energetically favorable.

LG basis combined with orthogonality [Eqs.(4c, 4b)]. Using Eq.(4a) one can estimate that for $|q_{max}| = 10^{-p}k_0$ and $\Delta z = 10^l \lambda_0$ the modal attenuation factor is $\exp\left(-2\pi 10^{l-2p}\right)$ which yields $\approx 94\%$ of the incoming photon flux at the output for $l = p = 2$. This geometry simulates the dynamics of the Hamiltonian $H_{eff}^{LG} = H_{UC}$,

$$H_{UC} = \sum_{\langle n,k \rangle \in \mathcal{D}_h} \Theta_{nk} a_n^\dagger a_k - \sum_{n,k \in \mathcal{D}_\Delta} \mathcal{U}_{nk}\hat{n}_n\hat{n}_k, \qquad (11)$$

where $\langle n, k \rangle$ stands for nearest neighbors. $\mathcal{D}_h$ is a domain determined by the geometry in which the hopping occurs, as shown in Fig.(4). $\mathcal{D}_\Delta$ is the domain set by Δ for which several illustrations are depicted in Fig.(2).

Discussion. We have developed a geometric SPC, shaping photon-photon interactions via geometric design of the coupling between spatial modes, using the setup depicted in Fig.(1). Quantum dynamics of interacting bosons described by the Hamiltonian of Eq.(1) can be simulated and directly measured using the above ingredients.

The dynamics of the SBs constrained by the Eq.(1) is controlled by the following three main quantities. The geometric distribution of molecules, their internal structure and the choice of spatial basis. The dynamics induced by the geometric SPC depicted in Fig.(3) can be restricted to a finite set of modes as demonstrated in Fig.(4). This offers a *purpose-computing platform* to a class of problems with exponential complexity. There is a growing interest in purpose machines, built for the solution of a specific task, e.g. coherent Ising machines [26, 27]. These

structures are designed to solve efficiently Ising models on graphs with programmable connectivity. Their usefulness stems from the well known mapping between the Ising model ground state search problem, and combinatorial optimization problems in polynomial time [28] (both NP hard). The proposed setup is also applicable as a quantum (light) state-preparation technique, as well as multi-photon gate in a photonic quantum processor.

In molecular systems the number of vibrational modes N_{vib} is proportional to the number of atoms N_a according to $N_{vib} = 3N_a - 6$. The number of electronic states corresponds to the number of electrons N_e. Good candidates would be systems containing few vibrational modes while large number of electrons that potentially provide strong coupling of the vibrational modes with applied electromagnetic field. Short wavelength tabletop X-ray sources that couple off-resonantly between the vibrational modes provide intriguing possibility for source realization [29]. Longer wavelength sources for which sophisticated measurement techniques are more mature may be possible although the coupling between the modes may take more complicated forms.

Due to the structure of the LG modes, for low number of ordered scatterers, sign-flipping anti-ferromagnetic coupling has been observed that requires further characterization. Finding the molecular distribution and basis emulating the desired dynamics provides a topic for future study as well as coupling to electronic states rather than the vibrational. For this purpose, another degree of the geometric properties could be considered, the local charge distribution of a each scatterer presented in Eqs.(7a,7b).

[*] Shahaf.S.Asban@gmail.com
[†] smukamel@uci.edu
[1] M. A. Nielsen and I. L. Chuang, *Quantum Computation and Quantum Information: 10th Anniversary Edition* (Cambridge University Press, 2010).
[2] Assuming voltage levels are assigned to bit states, having '0' represented by zero voltage.
[3] P. Massoud Salehi and J. Proakis, *Digital Communications* (McGraw-Hill Education, 2007).
[4] P. W. Shor, Scheme for reducing decoherence in quantum computer memory, Phys. Rev. A **52**, R2493 (1995).
[5] D. Gottesman, A. Kitaev, and J. Preskill, Encoding a qubit in an oscillator, Phys. Rev. A **64**, 12310 (2001).
[6] P. Schindler, J. T. Barreiro, T. Monz, V. Nebendahl, D. Nigg, M. Chwalla, M. Hennrich, and R. Blatt, Experimental Repetitive Quantum Error Correction, Science **332**, 1059 (2011).
[7] J. I. Cirac and P. Zoller, Quantum Computations with Cold Trapped Ions, Phys. Rev. Lett. **74**, 4091 (1995).
[8] D. Jaksch, C. Bruder, J. I. Cirac, C. W. Gardiner, and P. Zoller, Cold Bosonic Atoms in Optical Lattices, Phys. Rev. Lett. **81**, 3108 (1998).
[9] C. Monroe, Quantum information processing with atoms and photons, Nature **416**, 238 (2002).
[10] K. Kim, M.-S. Chang, S. Korenblit, R. Islam, E. E. Edwards, J. K. Freericks, G.-D. Lin, L.-M. Duan, and C. Monroe, Quantum simulation of frustrated Ising spins with trapped ions, Nature **465**, 590 (2010).
[11] M. Schreiber, S. S. Hodgman, P. Bordia, H. P. Lüschen, M. H. Fischer, R. Vosk, E. Altman, U. Schneider, and I. Bloch, Observation of many-body localization of interacting fermions in a quasirandom optical lattice, Science **349**, 842 (2015).
[12] J. Smith, A. Lee, P. Richerme, B. Neyenhuis, P. W. Hess, P. Hauke, M. Heyl, D. A. Huse, and C. Monroe, Many-body localization in a quantum simulator with programmable random disorder, Nature Physics **12**, 907 (2016).
[13] E. Zohar, J. I. Cirac, and B. Reznik, Quantum simulations of lattice gauge theories using ultracold atoms in optical lattices, Reports on Progress in Physics **79**, 14401 (2015).
[14] E. Rico, M. Dalmonte, P. Zoller, D. Banerjee, M. Bogli, P. Stebler, and U.-J. Wiese, So(3) "nuclear physics" with ultracold gases, Annals of Physics **393**, 466 (2018).
[15] C. Muschik, M. Heyl, E. Martinez, T. Monz, P. Schindler, B. Vogell, M. Dalmonte, P. Hauke, R. Blatt, and P. Zoller, U(1) wilson lattice gauge theories in digital quantum simulators, New Journal of Physics **19**, 103020 (2017).
[16] In linear order of the paraxiality parameter ϑ there are *no losses* in the longitudinal modes. Losses in the transverse modes are governed solely by the geometry. Higher orders exhibit losses and demonstrated in the illustration below.
[17] S. Asban, K. E. Dorfman, and S. Mukamel, Quantum phase-sensitive diffraction and imaging using entangled photons, Proceedings of the National Academy of Sciences **116**, 11673 (2019), https://www.pnas.org/content/116/24/11673.full.pdf.
[18] R. Fickler, G. Campbell, B. Buchler, P. K. Lam, and A. Zeilinger, Quantum entanglement of angular momentum states with quantum numbers up to 10,010, Proceedings of the National Academy of Sciences **113**, 13642 (2016), arXiv:1607.00922.
[19] R. Fickler, R. Lapkiewicz, W. N. Plick, M. Krenn, C. Schaeff, S. Ramelow, and A. Zeilinger, Quantum Entanglement of High Angular Momenta, Science **338**, 640 (2012).
[20] M. Krenn, R. Fickler, M. Huber, R. Lapkiewicz, W. Plick, S. Ramelow, and A. Zeilinger, Entangled singularity patterns of photons in Ince-Gauss modes, Phys. Rev. A **87**, 12326 (2013).
[21] J. Bavaresco, N. Herrera Valencia, C. Klöckl, M. Pivoluska, P. Erker, N. Friis, M. Malik, and M. Huber, Measurements in two bases are sufficient for certifying high-dimensional entanglement, Nature Physics **14**, 1032 (2018).
[22] S. S. Straupe, D. P. Ivanov, A. A. Kalinkin, I. B. Bobrov, and S. P. Kulik, Angular schmidt modes in spontaneous

parametric down-conversion, Phys. Rev. A **83**, 060302(R) (2011).

[23] Using entangled photon pair such that the as SB and RSB ideally results in background free signal yet harder to produce.

[24] A. Aiello and J. P. Woerdman, Exact quantization of a paraxial electromagnetic field, Phys. Rev. A **72**, 060101(R) (2005).

[25] G. F. Calvo, A. Picon, and E. Bagan, Quantum field theory of photons with orbital angular momentum, Phys. Rev. A **73**, 013805 (2006).

[26] T. Inagaki, Y. Haribara, K. Igarashi, T. Sonobe, S. Tamate, T. Honjo, A. Marandi, P. L. McMahon, T. Umeki, K. Enbutsu, O. Tadanaga, H. Takenouchi, K. Aihara, K.-i. Kawarabayashi, K. Inoue, S. Utsunomiya, and H. Take-

sue, A coherent Ising machine for 2000-node optimization problems, Science **354**, 603 (2016).

[27] P. L. McMahon, A. Marandi, Y. Haribara, R. Hamerly, C. Langrock, S. Tamate, T. Inagaki, H. Takesue, S. Utsunomiya, K. Aihara, R. L. Byer, M. M. Fejer, H. Mabuchi, and Y. Yamamoto, A fully programmable 100-spin coherent Ising machine with all-to-all connections, Science **354**, 614 (2016).

[28] F. Barahona, On the computational complexity of Ising spin glass models, Journal of Physics A: Mathematical and General **15**, 3241 (1982).

[29] J. J. Rocca, Table-top soft x-ray lasers, in *Conference on Lasers and Electro-Optics* (Optical Society of America, 2016) p. AM1K.1.